Ali, W.H., M.S. Bhabra, P.F.J. Lermusiaux, A. March, J.R. Edwards, K. Rimpau, and P. Ryu, 2019. Stochastic Oceanographic-Acoustic Prediction and Bayesian Inversion for Wide Area Ocean Floor Mapping. In: OCEANS '19 MTS/IEEE Seattle, 27-31 October 2019, doi:10.23919/OCEANS40490.2019.8962870

Stochastic Oceanographic-Acoustic Prediction and Bayesian Inversion for Wide Area Ocean Floor Mapping

Wael H. Ali[1], Manmeet S. Bhabra[1], Pierre F. J. Lermusiaux[†,1],
Andrew March[2], Joseph R. Edwards[2], Katherine Rimpau[2], Paul Ryu[2]
[1]*Department of Mechanical Engineering, Massachusetts Institute of Technology, Cambridge, MA*
[2]*Lincoln Laboratory, Massachusetts Institute of Technology, Lexington, MA*
[†]Corresponding Author: pierrel@mit.edu

***Abstract*—Covering the vast majority of our planet, the ocean is still largely unmapped and unexplored. Various imaging techniques researched and developed over the past decades, ranging from echo-sounders on ships to LIDAR systems in the air, have only systematically mapped a small fraction of the seafloor at medium resolution. This, in turn, has spurred recent ambitious efforts to map the remaining ocean at high resolution. New approaches are needed since existing systems are neither cost nor time effective. One such approach consists of a sparse aperture mapping technique using autonomous surface vehicles to allow for efficient imaging of wide areas of the ocean floor. Central to the operation of this approach is the need for robust, accurate, and efficient inference methods that effectively provide reliable estimates of the seafloor profile from the measured data. In this work, we utilize such a stochastic prediction and Bayesian inversion and demonstrate results on benchmark problems. We first outline efficient schemes for deterministic and stochastic acoustic modeling using the parabolic wave equation and the optimally-reduced Dynamically Orthogonal equations and showcase results on stochastic test cases. We then present our Bayesian inversion schemes and its results for rigorous nonlinear assimilation and joint bathymetry-ocean physics-acoustics inversion.**

***Index Terms*—Stochastic PDEs, Bayesian Inference, Gaussian Mixture Model—Dynamically Orthogonal (GMM-DO) filter, Ocean modeling, Acoustic Parabolic Equations, Generalized Tomography**

I. Introduction

Nearly 71% of the Earth is covered by the world's ocean, a total area corresponding to approximately 362 million square kilometers, yet only a small fraction has ever been mapped from direct observation [17]. Recent studies show that despite the large advances in methods used for seafloor mapping since it began in the 19th century, surprisingly, less than 18% of the ocean floor has been resolved at a resolution of less than 1 km [37]. In contrast, Earth's land masses have been mapped to a resolution of 30m or less, a difference that results from the fact that electromagnetic waves, which form the basis of light and radar terrestrial mapping systems, are severely attenuated in water and thus cannot be used for effective seabed imaging [20]. Ultimately, this lack of detailed bathymetry data is a major limitation in our ability to understand instrumental ocean and seafloor processes.

The importance of an accurate knowledge of the seafloor can hardly be overstated. It plays a significant role in augmenting our knowledge of geophysical and oceanographic phenomena, including ocean circulation patterns, tides, sediment transport, and wave action [16, 20, 41]. Ocean seafloor knowledge is also critical for safe navigation of maritime vessels as well as marine infrastructure development, as in the case of planning undersea pipelines or communication cables [20]. The importance of having a detailed understanding of the seafloor has resulted in a push in recent years for more concerted efforts to fill gaps in our limited bathymetric knowledge. One such initiative that has been launched is a joint effort by GEBCO and the Nippon Foundation known as the Seabed 2030 project, an ambitious venture to map the entire world ocean by the year 2030 [20, 37].

Modern bathymetric mapping techniques can broadly be classified as belonging to the class of either acoustic, optical, or radar approaches. First, due to the ability of sound to propagate large distances underwater with little attenuation relative to air, acoustic approaches have been used to resolve centimeter-to-kilometer scale underwater features. Commonly referred to as echo-sounding, initial acoustic bathymetry determination techniques were based on the basic idea of emitting a sound pulse and measuring the time taken for it to propagate toward the seafloor and reflect back to the surface. Single Beam Echo-Sounders follow this principle by using a transducer, typically mounted to the hull of the marine vessel, to generate and receive acoustic signals and then use corresponding travel time measurements to measure the depth. The limited seafloor coverage of the single beam echo-sounder spurred the development of the multibeam echo-sounder, the primary tool used for high-resolution acoustic mapping today. After first focusing sound into a wide swath or fan, multibeam echo-sounders use a series of hydrophones to detect the returning echoes in narrow strips perpendicular to the fan. With most systems achieving beam angles between 120 and 150 degrees, multibeam echo-sounders can effectively be used to map large patches of the seafloor using a single pass of the vessel. Moreover, the resolution of the resulting maps, for both the single and multibeam case, is inversely related to the water

978-0-578-57618-3

depth: for deeper water depths, although larger patches of the ocean are ensonified, the obtained map has a low resolution, whereas the opposite holds true in shallow regions. Although effective in obtaining high resolution maps, key disadvantages of single-beam and multibeam echo-sounders are the large amounts of time and high costs required for vessels to be deployed and take measurements [9, 25, 8, 7, 47].

Optical approaches have also been used extensively in seafloor mapping using visible light and either passive or active sensors. Passive optical sensors measure the reflected solar radiation from the seafloor by collecting data in a wide spectral band, ranging from the visible to the infrared portion of the electromagnetic spectrum. The reflected spectrum can then be used to effectively infer the unknown bathymetry. Active optical sensors, commonly known as light detecting and ranging (LIDAR) sensors, perform similar to echo-sounders in that they produce streams of light and measure the round-trip travel time to estimate the distance to the seafloor. LIDAR sensors, normally boarded on airborne platforms, traditionally use two lasers to infer the bathymetry. First an infrared laser, which does not penetrate into the water, is used to measure the sea surface, and then a second green laser, which penetrates into the water column, is used to determine the distance to the seafloor. Optical systems enjoy lower time and monetary costs, however, their use is restricted to shallow water regions, as visible light cannot penetrate effectively to deeper depths, and to areas with high water clarity [9, 19].

Radar systems belong to an additional, commonly-used class of seafloor mapping techniques. Satellite altimetry, one such prevalent technique, measures the ocean depth through studying the height of the ocean's surface which is influenced by—among other factors—the gravitational effects of topographic features on the seafloor. Using altimetry data and gravity models, large scale seabed features such as ridges and troughs, which exert non-negligible changes to the Earth's gravitational field, can be detected using this scheme but at a relatively low resolution [9, 55, 44, 43].

The aforementioned approaches, each with their advantages and disadvantages, highlight the difficulty in obtaining a cost-effective and high-resolution ocean floor mapping system. This has galvanized increased research into improved mapping techniques in the past decade [55]. One such approach—proposed and under development by the MIT Lincoln Laboratory—is the Wide Area Ocean Floor Mapping system. Using a novel sparse-aperture-mapping-technique consisting of autonomous surface vehicles, this system has the potential to effectively map the seabed in both a time-and-cost-effective manner.

Essential to the development of the sparse-aperture sonar system is the need for robust, accurate, and efficient inference schemes that can use measured data to accurately estimate the bathymetry and quantify the errors of these estimates. Central to obtaining this result are three major challenges that must be addressed. First, accurate and computationally efficient numerical schemes for deterministic acoustic modeling is required. We address this by highlighting our efficient numerical schemes for the 2D and 3D integration of the parabolic wave equation [24, 12]. Second, once the deterministic problem is dealt with, the effects of the inherent uncertainty in the acoustic and ocean environment must be accounted for by developing methods for solving the stochastic versions of the governing partial differential equations (PDEs). We thus develop probabilistic prediction schemes for solving the stochastic parabolic equation using the optimally-reduced Dynamically Orthogonal (DO) equations [1, 3]. The derived equations allow predicting probabilities for acoustic fields, fully respecting the nonlinear governing equations and non-Gaussian statistics of the uncertain environment parameter—in this work, the sound speed profile [45, 46, 13]. Finally, once the forward stochastic problem is solved, the third challenge concerns the development of schemes for rigorous assimilation and joint principled Bayesian inversion of environmental and acoustic fields to infer probabilistic posterior estimates of the bathymetry field. To do this, we utilize and extend our Gaussian Mixture Model DO (GMM-DO) filter and smoother schemes, which allow for novel PDE-based Bayesian inversion while combining the stochastic DO parabolic differential equation with GMMs and allowing for nonlinear, non-Gaussian estimation of the states and parameters [49, 48]. Using sparse acoustic measurements, we are thus able to show updated posteriors for the unknown bathymetry profile [1, 2].

This paper is organized as follows. In section II, we outline our methodology for efficient deterministic and stochastic acoustic modeling, and joint Bayesian bathymetry–ocean physics–acoustics inversion. In section III, we provide validation results for our implementation of the acoustic models. We then showcase our stochastic acoustic modeling and inversion results for a new benchmark test case, the uncertain bump problem. Conclusions are in section IV.

II. Methodology

A. Background on Underwater Acoustic Modeling

The equations governing the acoustic pressure field can be derived from the fundamental mass and momentum conservation laws by assuming that the sound waves introduce a small perturbation on the ocean pressure, density, and velocity fields. For an isotropic broadband point source with signal strength $S(t)$, these equations reduce to the acoustic wave equation [5]:

$$\rho\nabla\cdot\left(\frac{1}{\rho}\nabla p_t\right)-\frac{1}{c^2}\frac{\partial^2 p_t}{\partial t^2}=-S(t)\,\frac{2\delta\left(\boldsymbol{x}_\perp-\boldsymbol{x}_{\perp s}\right)\delta(\eta)}{\eta}\,, \quad (1)$$

subject to the appropriate initial and boundary conditions in the domain of interest. In this equation, ρ corresponds to the medium density, p_t is the time-domain acoustic pressure field, and c is the medium sound speed. In addition, Cartesian coordinates are used, and following the notation from [32], the position $\boldsymbol{x}\in\mathcal{D}\times[0,R]$ is written as $\boldsymbol{x}=(\boldsymbol{x}_\perp,\eta)$, with $\boldsymbol{x}_\perp\in\mathcal{D}$ denoting the two-dimensional transverse coordinates, and $\eta\in[0,R]$ denoting the position in the range direction, typically chosen as the largest dimension in the domain.

Finally, the isotropic time-harmonic point sound source is located at $\eta = 0$ and $\boldsymbol{x}_\perp = \boldsymbol{x}_{\perp,s}$.

For a time-harmonic point source with signal amplitude A and frequency ω_0, the signal spectrum is:

$$\hat{S}(\omega) = 2\pi A\, \delta(\omega - \omega_0). \tag{2}$$

Working in the frequency domain, the acoustic wave equation (1) reduces then to the Helmholtz equation [5]:

$$\rho\nabla\cdot\left(\frac{1}{\rho}\nabla p\right) + k_a^2 p = -\frac{2\delta(\boldsymbol{x}_\perp - \boldsymbol{x}_{\perp,s})\,\delta(\eta)}{\eta}, \tag{3}$$

where $p = p(\boldsymbol{x}_\perp, \eta)$ is the frequency-domain acoustic pressure field (appropriately normalized by the signal amplitude A), $k_a = \frac{\omega_0}{c}(1 + ia)$ is the complex (accounting for medium absorption) wave number where ω_0 corresponds to the source angular frequency, $c = c(\boldsymbol{x}_\perp, \eta)$ is the space-varying medium sound speed, and $a = a(\boldsymbol{x}_\perp, \eta)$ is the attenuation coefficient. Furthermore, we are commonly interested in solving the PD (3) to compute the transmission loss (TL) field given by,

$$TL(\boldsymbol{x}_\perp, \eta) = -20\log\left|\frac{p(\boldsymbol{x}_\perp, \eta)}{p_0(\eta = 1)}\right|, \tag{4}$$

where $p_0(\eta = 1)$ is a nominal pressure value [24].

Solving the elliptic Helmholtz equation (3) in large domains typically encountered in underwater acoustics is computationally expensive. Several solution techniques have been proposed to address this challenge, and these can be grouped under five categories: Ray Theory, Normal Mode, Multipath Expansion, Wavenumber Integration (Fast Field) and Parabolic Equation (PE) Methods [24]. Each of these techniques has its domain of applicability according to the acoustic frequency and environmental complexity [12].

In this work, relatively low frequency acoustic problems where the medium properties vary with range are of interest. As a result, the parabolic equation (PE) method is adopted. Under the parabolic equation (PE) approximation [52, 34], the acoustic pressure $p(\boldsymbol{x}_\perp, \eta)$ can be decomposed as,

$$p(\boldsymbol{x}_\perp, \eta) = v(\eta)\,\psi(\boldsymbol{x}_\perp, \eta), \tag{5}$$

where $v(\eta)$ is a function strongly dependent on the range direction η, and the envelope function $\psi(\boldsymbol{x}_\perp, \eta)$ denotes the outgoing complex acoustic field and is only weakly dependent on η.

With appropriate choice of the separation constant, and by further assuming that backscattering effects in range are negligible (this can be justified when the medium properties only vary slowly with range), the functions $v(\eta)$ and $\psi(\boldsymbol{x}_\perp, \eta)$ can be found to satisfy [24],

$$\begin{aligned} &v(\eta) \sim \exp(ik_0\eta), \\ &\frac{\partial}{\partial\eta}\psi(\boldsymbol{x}_\perp, \eta) = \\ &ik_0\left\{\sqrt{\mathbf{I} + (n_a^2 - 1)\mathbf{I} + \frac{1}{k_0^2}\rho\nabla_\perp\cdot\left(\frac{1}{\rho}\nabla_\perp\right)} - \mathbf{I}\right\}\psi(\boldsymbol{x}_\perp, \eta), \end{aligned} \tag{6}$$

where $k_0 = \omega_0/c_{ref}$, with c_{ref} a reference sound speed. In addition, $\mathbf{I}$ is the identity operator, n_a is the index of refraction defined as,

$$n_a^2(\boldsymbol{x}_\perp, \eta) = \left(\frac{c_{ref}}{c(\boldsymbol{x}_\perp, \eta)}\right)^2\left(1 + i\frac{a(\boldsymbol{x}_\perp, \eta)}{27.29}\right), \tag{7}$$

and $\rho\nabla_\perp\cdot\left(\frac{1}{\rho}\nabla_\perp\right)$ is the 2-D Laplacian-like operator, defined as,

$$\rho\nabla_\perp\cdot\left(\frac{1}{\rho}\nabla_\perp\right) = \rho\frac{\partial}{\partial x_1}\left(\frac{1}{\rho}\frac{\partial}{\partial x_1}\right) + \rho\frac{\partial}{\partial x_2}\left(\frac{1}{\rho}\frac{\partial}{\partial x_2}\right), \tag{8}$$

where $\boldsymbol{x}_\perp = (x_1, x_2)$ are the transverse coordinates.

Given that the medium sound speed field does not vary significantly with range, the PE approach becomes significantly more computationally efficient as the 3-D elliptic-type (3) has been reduced to a parabolic-type (6), which can be solved by marching along the range direction η with an acceptable accuracy [12, 24].

In what follows, the operator $\mathbf{Q}$ is used to denote

$$\mathbf{Q} = (n_a^2 - 1)\mathbf{I} + \frac{1}{k_0^2}\rho\nabla_\perp\cdot\left(\frac{1}{\rho}\nabla_\perp\right), \tag{9}$$

and the PE is rewritten as

$$\frac{\partial}{\partial\eta}\psi(\boldsymbol{x}_\perp, \eta) = ik_0\left\{\sqrt{\mathbf{I} + \mathbf{Q}} - \mathbf{I}\right\}\psi(\boldsymbol{x}_\perp, \eta). \tag{10}$$

Within the PE solution technique, computing the square root operator $\sqrt{\mathbf{I} + \mathbf{Q}}$ is generally nontrivial. This corresponds to computing the square root of a matrix in discrete sense, which is known to be challenging: it might not exist, might not be unique, and might not be a function of the operator itself [18]. Several methods have been used to approximate the square root operator, among these are: (i) Taylor-series based methods [52, 50, 33], and (ii) Padé-series based methods [51, 6].

An example of a Taylor-series based PE is the standard narrow-angle PE (NAPE), which is the most widely used within the acoustics community [52]. It can be derived by retaining one term in the Taylor series approximation of the square root operator

$$\sqrt{\mathbf{I} + \mathbf{Q}} \approx \mathbf{I} + \frac{1}{2}\mathbf{Q}. \tag{11}$$

The NAPE is then obtained as

$$\frac{\partial}{\partial\eta}\psi(\boldsymbol{x}_\perp, \eta) = \left\{\frac{ik_0}{2}(n_a^2 - 1) + \frac{i}{2k_0}\rho\nabla_\perp\cdot\left(\frac{1}{\rho}\nabla_\perp\right)\right\}\psi(\boldsymbol{x}_\perp, \eta), \tag{12}$$

which is a reaction-diffusion like equation. Due to truncation in the Taylor series, this equation is only valid for computing propagation at an angle ± 15 degrees around the source, and hence the name narrow-angle [52, 24].

On the other hand, Padé-series based PE [51] can be derived by approximating the square root operator

$$\sqrt{\mathbf{I} + \mathbf{Q}} \approx \mathbf{I} + \sum_{j=1}^{m}\frac{a_{j,m}\mathbf{Q}}{\mathbf{I} + b_{j,m}\mathbf{Q}}, \tag{13}$$

where the truncation of the series to order m yields wider angle of applicability. For instance, $m = 1$ corresponds to the Claerbout WAPE [6] with ± 55 degrees propagation angle. The coefficients are moreover given as

$$a_{j,m} = \frac{2}{2m+1} \sin^2\left(\frac{j\pi}{2m+1}\right), b_{j,m} = \cos^2\left(\frac{j\pi}{2m+1}\right). \tag{14}$$

The Padé WAPE (Pa-WAPE) are then obtained as

$$\frac{\partial}{\partial \eta}\psi(\boldsymbol{x}_\perp, \eta) = \left\{ ik_0 \sum_{j=1}^{m} \left(\mathbf{I} + b_{j,m}\mathbf{Q}\right)^{-1} a_{j,m}\mathbf{Q} \right\} \psi(\mathbf{x}_\perp, \eta). \tag{15}$$

B. Efficient Techniques for Deterministic Modeling

Several challenges arise when modeling the underwater acoustic propagation using the NAPE and Pa-WAPE. Specifically, acoustic applications typically require modeling propagation over large domains leading to memory limitations in assembling and storing the corresponding matrix discretizations. Also, 3D acoustic propagation problems lead to large bandwidth in the corresponding discrete linear systems. Lastly, Pa-WAPE specifically suffers from the need to invert the operator $(\mathbf{I} + b_{j,m}\mathbf{Q})$ on the right-hand side of equation (15), limiting its application to orders of $m = 1, 2$.

Presently, we address these challenges by implementing the NAPE and Pa-WAPE within a finite volume (FV) framework [54]. Second-order spatial FV schemes are used to discretize the right-hand side in the transverse physical space $\mathcal{D}$, and a second-order backward difference scheme is used to march the solution in range. The implementation makes use of matrix-free, operational and dimensional splitting techniques leading to lower memory requirements, smaller bandwidth in the discrete linear systems, and faster performance [1].

The initial conditions at range $\eta = 0$ are typically provided using analytical or numerical techniques based on other acoustic models. In this work, Gaussian and Greene analytical starters are used to initialize the PE equations [24]. Furthermore, the equations are subject to a pressure-release boundary condition, *i.e.* Dirichlet zero, at the free surface, while artificial absorption layers are introduced on the remaining boundaries to eliminate spurious wave reflections introduced by truncating the domain. Further details about the implementation of these initial and boundary conditions can be found in [24].

To validate our implementation, we compare predictions of the acoustic field in benchmark test cases against those obtained using KRAKEN, a widely used normal mode model for range-dependent environments through adiabatic or full forward mode coupling [40]. The comparisons are discussed in the results Section III.

C. Coupled Oceanographic-Acoustic-Bathymetry Probabilistic Modeling

In this work, we parametrize the incomplete knowledge about the bathymetry and the ocean environment through uncertainties in the sound speed field, and we represent it as a stochastic field $c(\boldsymbol{x}_\perp, \eta; \xi)$, where $\xi \in \Xi$, with Ξ a measurable sample space equipped with an appropriate σ-algebra $\mathcal{F}$ and probability measure μ.

In what follows, we present our methodology for modeling these uncertainties for the case of NAPE, which is now generalized to the following stochastic PDE (SPDE):

$$\begin{aligned} \frac{\partial \psi(\boldsymbol{x}_\perp, \eta; \xi)}{\partial \eta} =& \mathcal{L}\left[\psi(\boldsymbol{x}_\perp, \eta; \xi); \xi\right], \\ & \boldsymbol{x}_\perp \in \mathcal{D},\ \eta \in [0, R],\ \xi \in \Xi, \end{aligned} \tag{16}$$

where $\mathcal{L}$ is the stochastic NAPE operator defined as

$$\begin{aligned} &\mathcal{L}\left[\psi(\boldsymbol{x}_\perp, \eta; \xi); \xi\right] = \\ &\left\{ \frac{ik_0}{2}\left(n_a^2(\boldsymbol{x}_\perp, \eta; \xi) - 1\right) + \right. \\ &\left. \frac{i}{2k_0}\rho\nabla_\perp \cdot \left(\frac{1}{\rho}\nabla_\perp\right) \right\} \psi(\boldsymbol{x}_\perp, \eta; \xi). \end{aligned} \tag{17}$$

In this SPDE, the uncertain sound speed field $c(\boldsymbol{x}_\perp, \eta; \xi)$, and hence the uncertain index of refraction field $n_a(\boldsymbol{x}_\perp, \eta; \xi)$, act as a source of uncertainty in the predicted acoustic field $\psi(\boldsymbol{x}_\perp, \eta; \xi)$.

In order to model these uncertainties accurately and at reduced computational cost, we utilize the new optimally-reduced Dynamically Orthogonal (DO) acoustics differential equations derived in [1]. These acoustic DO equations are based on a dynamic model-order reduction for uncertainty quantification [45, 46, 13]. The stochastic index of refraction $\left(n_a^2(\boldsymbol{x}_\perp, \eta; \xi) = H(\boldsymbol{x}_\perp, \eta; \xi)\right)$ and acoustic $(\psi(\boldsymbol{x}_\perp, \eta; \xi))$ fields are represented as range-evolving DO decompositions,

$$\begin{aligned} H(\boldsymbol{x}_\perp, \eta; \xi) &= \bar{H}(\boldsymbol{x}_\perp, \eta) + \sum_{l=1}^{n_{s,H}} \tilde{H}_l(\boldsymbol{x}_\perp, \eta)\, \beta_l(\eta; \xi), \\ \psi(\boldsymbol{x}_\perp, \eta; \xi) &= \bar{\psi}(\boldsymbol{x}_\perp, \eta) + \sum_{i=1}^{n_{s,\psi}} \tilde{\psi}_i(\boldsymbol{x}_\perp, \eta)\, \alpha_i(\eta; \xi), \end{aligned} \tag{18}$$

where $\bar{H}(\boldsymbol{x}_\perp, \eta)$ and $\bar{\psi}(\boldsymbol{x}_\perp, \eta)$ are the mean fields, and $\tilde{H}_l(\boldsymbol{x}_\perp, \eta)$ and $\tilde{\psi}_i(\boldsymbol{x}_\perp, \eta)$ are orthonormal modes that form an ordered basis for the stochastic subspace of size $n_{s,H}$ and $n_{s,\psi}$, respectively. In addition, $\beta_l(\eta; \xi)$ and $\alpha_i(\eta; \xi)$ are zero-mean stochastic processes.

Predictive equations for the evolution of the mean, modes, and stochastic coefficients of the acoustic field ψ can be derived by substituting these decompositions into the governing PDEs. Further details about these equations and their numerical implementation can be found in [1].

Advantages over other methods in stochastic acoustic modeling, namely Monte Carlo (MC) sampling [15], Error Subspace Statistical Estimation (ESSE) [30, 42, 27, 31], Probability Density Function (PDF) propagation [21], Field Shifting (FS) [11, 22] and Polynomial Chaos (PC) expansion techniques [26, 14], include an instantaneously-optimal dynamic reduction, nonlinear governing equations for the DO decomposition, rich non-Gaussian statistics equivalent to large MC ensembles, and relatively low computational costs.

D. Nonlinear Bayesian Data Assimilation for Joint Oceanographic-Acoustic-Bathymetry Inversion

Now that we have developed capabilities for modeling the uncertainties in ocean physics, bathymetry, and acoustics environments, we address the challenge of predicting the posterior distribution of the bathymetry field from acoustic field and transmission loss measurements. This is done using our principled nonlinear Bayesian data assimilation (DA) [49, 48, 36, 35], which combines DO equations with Gaussian mixture models (GMMs). The adaptive stochastic DO equations presented in the previous section are employed to predict prior probability distributions for the full joint dynamical state. At ranges where acoustic measurements are collected, the DO subspace realizations are fit to semiparametric GMMs using the Expectation-Maximization algorithm and the Bayesian Information Criterion. Bayes' law is then efficiently carried out analytically within the evolving stochastic subspace. Instead of covariance functions, it is information-theoretic concepts such as mutual information among state variables and other relevant attributes that are employed in such Bayesian updates.

Advantages of this approach over other ocean acoustic tomography methods [38, 53, 10, 4] include the abilities to capture nonlinearities and non-Gaussian distributions and to provide joint/multivariate corrections to the probability distributions of the ocean physics, bathymetry and acoustics. This is also done at a lower computational cost as the DA is done in the reduced subspace obtained from the DO evolution equations. THe GMM-DO ocean-physics-acoustics filter extends the ESSE filter [29, 42, 28] to non-Gaussian DA.

III. Results

A. Benchmarking Results for Deterministic Underwater Acoustics

Our implementation of the deterministic NAPE and PaWAPE, the MIT MSEAS parabolic equation (PE) solver [1], is validated against KRAKEN [40], a normal-mode commercial acoustic code for two test cases: (1) a deterministic Pekeris waveguide with penetrable bottom, and (2) a deterministic 2D wedge propagation benchmark problem.

1) Deterministic Pekeris Waveguide with Penetrable Bottom: The first benchmark case is the deterministic Pekeris waveguide with penetrable bottom [39, 24]. It is a 2D shallow water test case with a point sound source located at depth $z = 50$ m and range $\eta = 0$ and emitting at a harmonic frequency $f = 250$ Hz. The waveguide is modeled as an isospeed sound channel with a sound speed $c_w = 1500$ m/s and a density $\rho_w = 1000$ kg/m^3. The bottom is characterized by a sound speed $c_b = 1550$ m/s, a density $\rho_b = 1200$ kg/m^3, and an attenuation $a_b = 1$ dB/λ. A description of the case is provided in Figure 1.

Comparisons of the TL field predictions by our MSEAS PE solver and KRAKEN are shown in Figure 2. A plot of the TL at a receiver depth $z_r = 50$ m is also shown in Figure 3. Both Figures show very good agreement between the two solvers, hence validating the implementation of the NAPE.

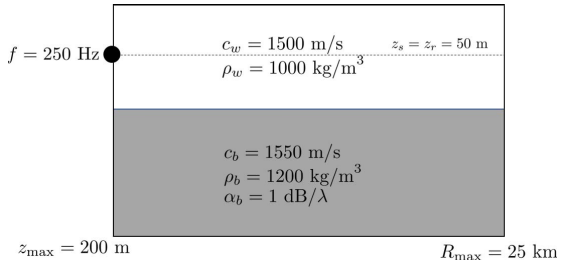

Fig. 1: Model domain for the deterministic Pekeris waveguide benchmark problem. A point sound source is located at depth $z = 50$ m and range $\eta = 0$ and emits at a harmonic frequency $f = 250$ Hz. The waveguide is modeled as an isospeed sound channel with sound speed $c_w = 1500$ m/s and density $\rho_w = 1000$ kg/m^3. The bottom is characterized by a sound speed $c_b = 1550$ m/s, a density $\rho_b = 1200$ kg/m^3, and an attenuation $a_b = 1$ dB/λ.

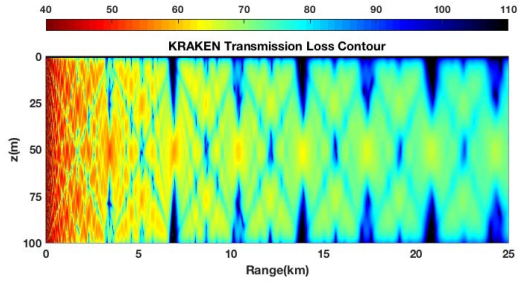

(a)

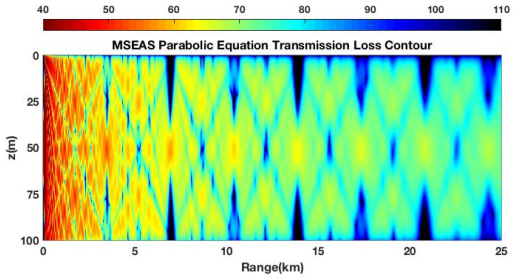

(b)

Fig. 2: Comparison of the transmission loss field predictions obtained by KRAKEN, a commercial acoustic solver, and by the developed MSEAS PE solver for the deterministic Pekeris waveguide problem. The predictions show very good agreement validating our implementation of the NAPE.

2) Deterministic 2D Wedge Propagation: The second benchmark is the deterministic 2D wedge propagation problem [23]. It is a 2D range dependent shallow water test case with a point sound source located at depth $z = 100$ m and range $\eta = 0$ and emitting at a harmonic frequency $f = 25$ Hz. The waveguide is modeled as an isospeed sound channel with a sound speed $c_w = 1500$ m/s and a density $\rho_w = 1000$ kg/m^3. The sloping bottom is characterized by a sound speed $c_b = 1700$ m/s, a density $\rho_b = 1500$ kg/m^3, and

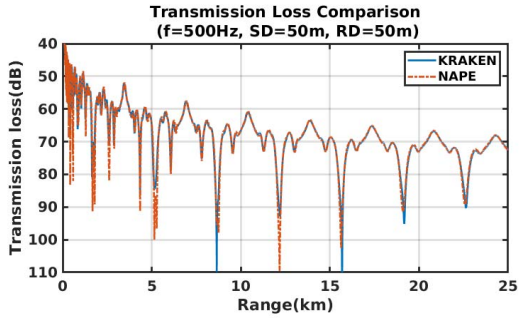

Fig. 3: Comparison of the transmission loss prediction at a receiver depth $z_r = 50$ m obtained by KRAKEN, a commercial acoustic solver, and the developed MSEAS PE solver for the deterministic Pekeris waveguide problem.

an attenuation $a_b = 0.5$ dB/λ. A description of the case is provided in Figure 4.

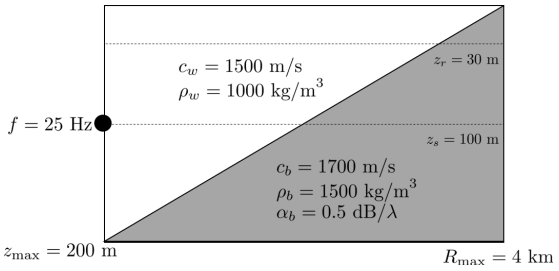

Fig. 4: Model domain for the deterministic 2D wedge propagation problem. A point sound source is located at depth $z = 100$ m and range $\eta = 0$ and emits at a harmonic frequency $f = 25$ Hz. The waveguide is modeled as an isospeed sound channel with sound speed $c_w = 1500$ m/s and density $\rho_w = 1000$ kg/m^3. The sloping bottom is characterized by a sound speed $c_b = 1700$ m/s, a density $\rho_b = 1500$ kg/m^3, and an attenuation $a_b = 0.5$ dB/λ.

Comparisons of the TL field predictions by our MSEAS PE solvers and KRAKEN are shown in Figure 5. A plot of the TL at a receiver depth $z_r = 30$ m is also shown in Figure 6. Both Figures show very good agreement between the two solvers, hence further validating our implementation.

B. Stochastic Acoustic-Bathymetry Predictions and Inversion Results in an Uncertain Bathymetry–Bump Test Case

In what follows, we showcase our modeling and assimilation techniques for a new benchmark test case, the uncertain bathymetry–bump problem.

1) Case Description: This test case is a stochastic extension of the deterministic Pekeris waveguide problem with penetrable bottom [39, 24] with a bump of width 100 m and height 15 m (represented using a cubic spline). It is a range dependent case where the sound speed and bathymetry vary with position along the range. The purpose of this test case is to test the capability of the developed technique in handling uncertain sound speed and bathymetry range dependencies,

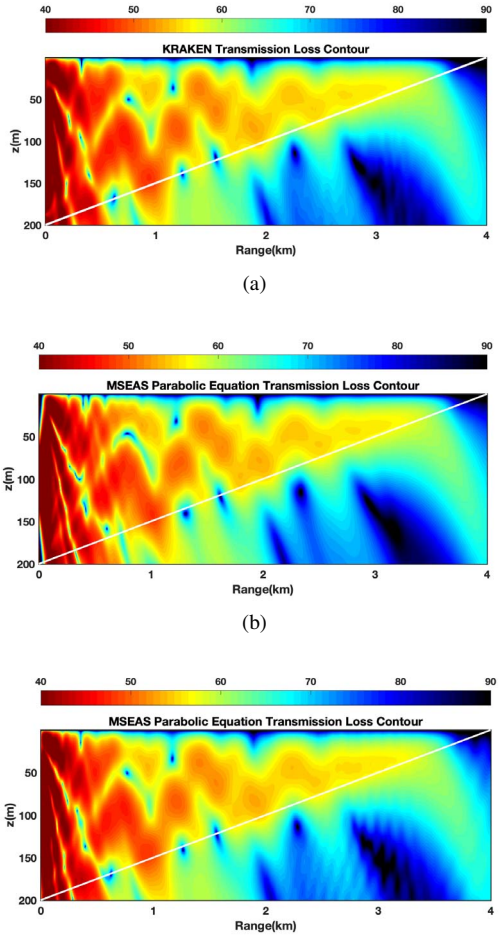

(a)

(b)

(c)

Fig. 5: Comparison of the transmission loss field predictions obtained by (a) KRAKEN, a commercial acoustic solver, and by (b-c) the developed MSEAS NAPE and Pa-WAPE solvers for the 2D wedge benchmark problem. The predictions show very good agreement validating our implementation.

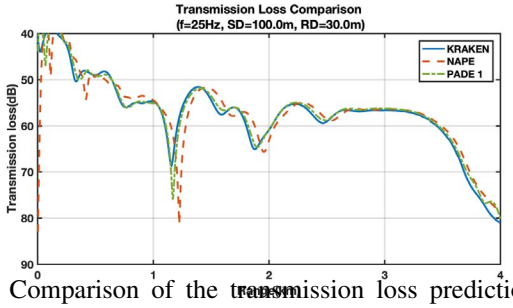

Fig. 6: Comparison of the transmission loss prediction at a receiver depth $z_r = 30$ m obtained by KRAKEN, a commercial acoustic solver, and the developed MSEAS NAPE and Pa-WAPE solvers for the 2D wedge benchmark problem.

and in providing corrections up to few meters accuracy, as required by the Wide Area Ocean Floor Mapping technology.

A point sound source is located at depth $z = 3$ m and range

$\eta = 0$ and emits at a harmonic frequency $f = 250$ Hz. The bottom is characterized by a sound speed $c_s = 1700$ m/s, a density $\rho_s = 1200$ kg/m^3, and an attenuation $a = 0.5$ dB/λ.

The background depth and the range location of the bump in this case are assumed uncertain, and are modeled probabilistically as two independent Gaussian random variable with mean positions $\mu_d = 100$ m, $\mu_r = 2$ km and standard deviations $\sigma_d = 20$ m, $\sigma_r = 50$ m. A description of the test case is provided in Figure 7 along with the resulting mean and standard deviation sound speed fields.

2) Stochastic Acoustic Predictions: The stochastic sound-speed-bathymetric environment is then input to our stochastic DO-NAPE model. It provides efficient and accurate predictions of the probability distributions of the acoustic transmission loss field. In Figure 8, we show these DO predictions for the uncertain TL field, specifically, the statistical mean, standard deviation, and the first 2 spatial DO modes. Significant uncertainty is located near the bathymetry, as expected. In addition, due to the bump's range location uncertainty, the spatial modes feature complex range dependencies.

3) Bayesian Bathymetry Inversion: Using the extended GMM-DO schemes for the joint ocean physics and acoustic Bayesian inversion, we assimilate sparse TL measurements collected at 3.5 km in range (10 observation locations shown as stars) to jointly update the TL (Figure 9), bathymetry, and sound speed fields (Figures 10 and 11). Specifically, Figure 9 shows the corrections obtained in the TL field upon assimilating the 10 sparse observations at the 3.5 km range. In Figure 10, we illustrate the true bathymetry overlaid on the prior and posterior sound speed fields. The Figure shows that, upon GMM-DO assimilation of the sparse TL observations, we jointly correct the background depth of the seafloor, the range location of the bump (highlighted in the plot of the zoomed region around it), and the sound speed field. This can be further explained by Figure 11 where we show differences in the mean prior and posterior sound speed fields from the truth.

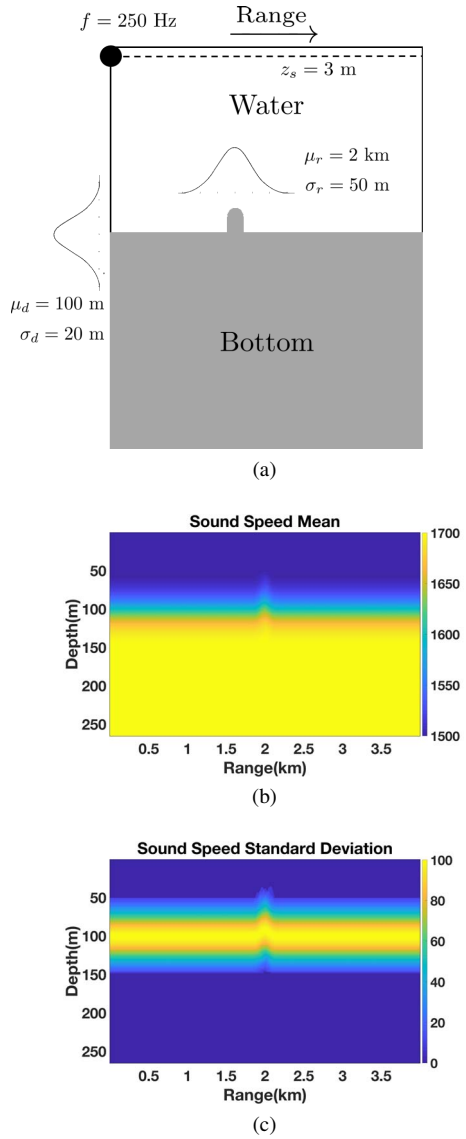

Fig. 7: Model domain, mean, and standard deviation sound speed fields for the uncertain bathymetry–bump test case. (a) A point sound source is located near the surface at depth $z = 3$ m and range $\eta = 0$, and emits at a harmonic frequency $f = 250$ Hz. A bell-shaped bump of width 100 m and height 15 m is located on the seafloor at an uncertain background depth and uncertain range location, parameterized by two independent Gaussian random variables with mean positions $\mu_d = 100$ m, $\mu_r = 2$ km and standard deviations $\sigma_d = 20$ m, $\sigma_r = 50$ m. (b-c) Resulting mean and standard deviation sound speed fields computed from 1000 ensemble realizations of the bump and seafloor locations.

IV. Conclusion

In this paper, we developed and validated a novel PDE-based methodology i) for predicting stochastic acoustic wave propagation in uncertain ocean-bathymetry environments, and ii) for the joint nonlinear Bayesian inversion of sound speed and bathymetry profiles from limited observations. We first reviewed background details on underwater acoustic modeling, and then presented efficient numerical techniques for deterministic modeling and validated our implementation for benchmark problems. We then discussed our method for handling uncertain bathymetry and sound speed fields using the optimally-reduced DO acoustic equations and then assimilating sparse observations using our nonlinear Bayesian GMM-DO filter. We showcased the developed methodology using a new stochastic acoustic benchmark test case, the uncertain bathymetry-bump problem. We find that the stochastic TL predictions are efficient and that the GMM-DO filter accurately and jointly corrects the TL, sound speed, and bathymetry fields from sparse TL measurements.

As the methodology is not limited to the NAPE formulation, this work can be extended to the Pa-WAPE, which would allow modeling propagation in steeper bathymetry environments. Further extensions include applications in more complex

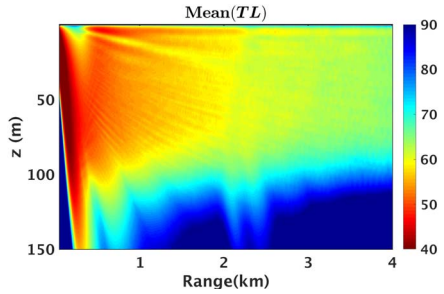

(a)

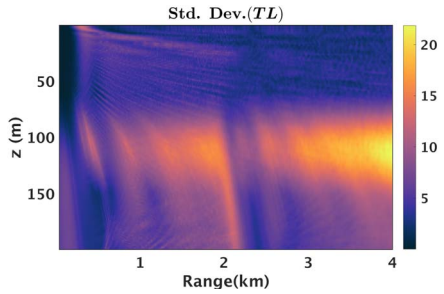

(b)

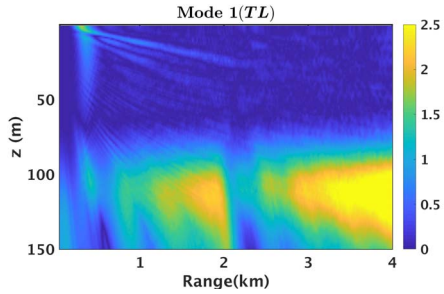

(c)

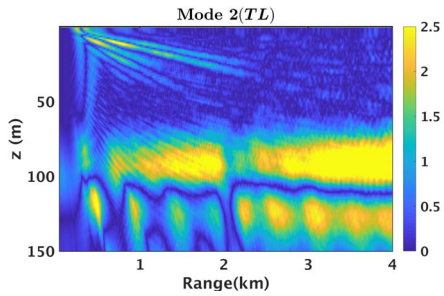

(d)

Fig. 8: DO solution for the stochastic TL field in the uncertain bathymetry–bump test case. The mean, standard deviation, and modes 1 and 2 (out of the 30 modes retained in the truncation) of the TL field are shown. Uncertainty in the TL field is mostly located near the bathymetry and has complex range dependencies, with an overall increase with range and variations due to the uncertain bump.

bathymetry and realistic ocean environments. In addition, the Bayesian learning technique presented here can be extended to geoacoustics inversion, whereby the acoustic measurements

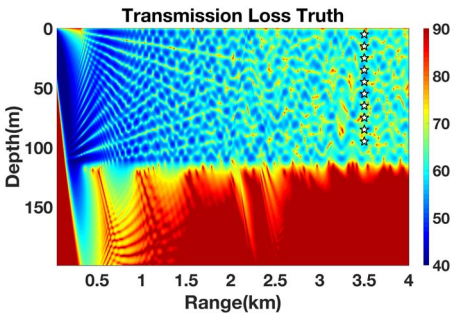

(a)

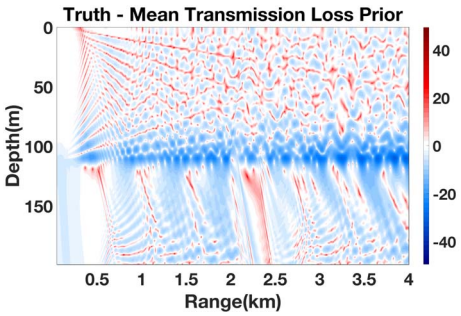

(b)

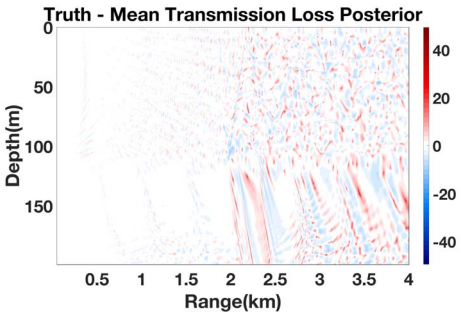

(c)

Fig. 9: Corrections of TL fields from assimilated sparse TL data. (a) Truth TL field from which 10 sparse measurements are collected (10 stars). (b-c) Differences between prior and posterior TL means (as predicted by the DO PE and GMM-DO assimilation framework, respectively) and the truth TL field in (a). Corrections in both water and bottom are clearly visible.

are used to infer the seabed properties. This is of particular importance in ocean floor mapping applications, and is the subject of our ongoing research.

ACKNOWLEDGMENTS

We thank the members of the MSEAS group for useful discussions. We are grateful to the Technology Office at MIT Lincoln Laboratory. We thank the Defense Advanced Research Projects Agency (DARPA) for support under grant N66001-16-C-4003 (POSYDON). PFJL also thanks the Office of Naval Research (ONR) for support under grants N00014-14-1-0725 (Bays-DA) and N00014-19-1-2693 (IN-BDA) to the Massachusetts Institute of Technology.

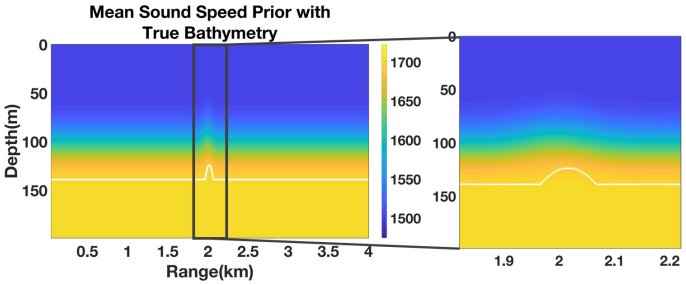

(a)

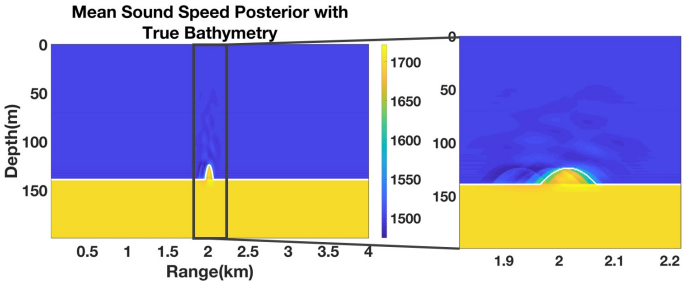

(b)

Fig. 10: Prior and posterior sound speed and bathymetry fields. (a) Prior sound speed mean with true bathymetry over the domain and zooming near the bump. (b) Posterior sound speed mean with true bathymetry over the domain and zooming near the bump. Corrections in the bump's depth and range locations upon assimilation of sparse TL observations (shown as 10 stars on the truth TL field in Figure 9) are clearly visible.

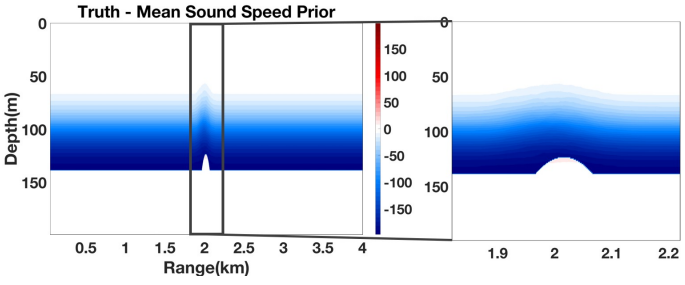

(a)

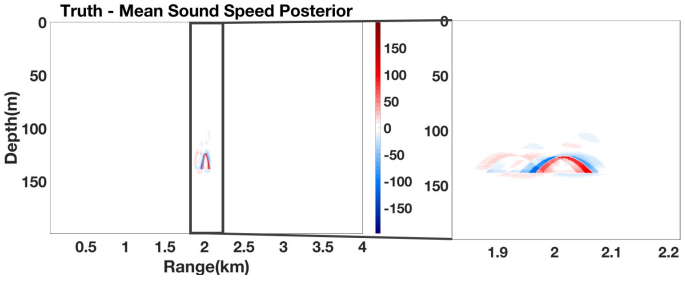

(b)

Fig. 11: Prior and posterior sound speed error fields. (a) Difference between the truth and mean prior sound speed field over the domain and zooming near the bump. (b) Difference between the truth and mean posterior sound speed field over the domain and zooming near the bump. Corrections in the sound speed field upon assimilating sparse TL measurements are clearly visible in both water and bottom.

References

[1] Wael H. Ali. Dynamically orthogonal equations for stochastic underwater sound propagation. Master's thesis, Massachusetts Institute of Technology, Computation for Design and Optimization Program, Cambridge, Massachusetts, September 2019.

[2] Wael H. Ali and Pierre F. J. Lermusiaux. Acoustics bayesian inversion with gaussian mixture models using the dynamically orthogonal field equations. 2019. In preparation.

[3] Wael H. Ali and Pierre F. J. Lermusiaux. Dynamically orthogonal equations for stochastic underwater sound propagation: Theory, schemes and applications. 2019. In preparation.

[4] Arthur B Baggeroer and William A Kuperman. Matched field processing in ocean acoustics. In *Acoustic Signal Processing for Ocean Exploration*, pages 79–114. Springer, 1993.

[5] Leonid M Brekhovskikh and Oleg A Godin. *Acoustics of layered media II: point sources and bounded beams*, volume 10. Springer Science & Business Media, 2013.

[6] Jon F Claerbout. *Fundamentals of geophysical data processing*. Citeseer, 1985.

[7] Keir Colbo, Tetjana Ross, Craig Brown, and Tom Weber. A review of oceanographic applications of water column data from multibeam echosounders. *Estuarine, coastal and shelf science*, 145:41–56, 2014.

[8] Christian De Moustier and Haruyoshi Matsumoto. Seafloor acoustic remote sensing with multibeam echo-sounders and bathymetric sidescan sonar systems. *Marine Geophysical Researches*, 15(1):27–42, 1993.

[9] Heidi M Dierssen and Albert E Theberge. Bathymetry: Assessing methods. *Encyclopedia of Ocean Sciences*, 2014.

[10] Stan E Dosso and Jan Dettmer. Bayesian matched-field geoacoustic inversion. *Inverse Problems*, 27(5):055009, 2011.

[11] Stan E. Dosso, Michael G. Morley, Peter M. Giles, Gary H. Brooke, Diana F. McCammon, Sean Pecknold, and Paul C. Hines. Spatial field shifts in ocean acoustic environmental sensitivity analysis. *J. of the Acoustical Society of America*, 122(5):2560–2570, 2007.

[12] Paul C Etter. *Underwater acoustic modeling and simulation*. CRC press, 2018.

[13] Florian Feppon and Pierre F. J. Lermusiaux. A geometric approach to dynamical model-order reduction. *SIAM Journal on Matrix Analysis and Applications*, 39(1):510–538, 2018.

[14] Steven Finette. A stochastic representation of environmental uncertainty and its coupling to acoustic wave propagation in ocean waveguides. *J. of the Acoustical Society of America*, 120(5):2567–2579, 2006.

[15] Peter Gerstoft and Christoph F Mecklenbräuker. Ocean acoustic inversion with estimation of a posteriori probability distributions. *J. of the Acoustical Society of America*, 104(2):808–819, 1998.

[16] Sarah T Gille. Bathymetry and ocean circulation. *Charting the Secret World of the Ocean Floor. The Gebco Project 1903.*

[17] John K Hall. Gebco centennial special issue–charting the secret world of the ocean floor: the gebco project 1903–2003. *Marine Geophysical Researches*, 27(1):1–5, 2006.

[18] Nicholas J Higham. Computing real square roots of a real matrix. *Linear Algebra and its applications*, 88:405–430, 1987.

[19] Jennifer L Irish and TE White. Coastal engineering applications of high-resolution lidar bathymetry. *Coastal engineering*, 35(1-2):47–71, 1998.

[20] M Jakobsson, G Allen, SM Carbotte, R Falconer, V Ferrini, K Marks, L Mayer, M Rovere, TW Schmitt, P Weatherall, et al.

The Nippon Foundation GEBCO seabed 2030: Roadmap for future ocean floor mapping. *Nippon Foundation-GEBCO*, 2030, 2017.

[21] Kevin R. James and David R. Dowling. A probability density function method for acoustic field uncertainty analysis. *J. of the Acoustical Society of America*, 118(5):2802–2810, 2005.

[22] Kevin R. James and David R. Dowling. A method for approximating acoustic-field-amplitude uncertainty caused by environmental uncertainties. *J. of the Acoustical Society of America*, 124(3):1465–1476, 2008.

[23] Finn B. Jensen and Carlo M. Ferla. Numerical solutions of range dependent benchmark problems in ocean acoustics. *JASA*, 87(4):1499–1510, 1990.

[24] Finn B Jensen, William A Kuperman, Michael B Porter, and Henrik Schmidt. *Computational ocean acoustics*. Springer Science & Business Media, 2011.

[25] Timothy A Kearns and Joe Breman. Bathymetry-the art and science of seafloor modeling for modern applications. *Ocean globe*, pages 1–36, 2010.

[26] Yu Yu Khine, Dennis B. Creamer, and Steven Finette. Acoustic propagation in an uncertain waveguide environment using stochastic basis expansions. *Journal of Computational Acoustics*, 18(04):397–441, 2010.

[27] P. F. J. Lermusiaux. Uncertainty estimation and prediction for interdisciplinary ocean dynamics. *Journal of Computational Physics*, 217(1):176–199, 2006.

[28] P. F. J Lermusiaux. Adaptive modeling, adaptive data assimilation and adaptive sampling. *Physica D: Nonlinear Phenomena*, 230(1):172–196, 2007.

[29] P. F. J. Lermusiaux and C.-S. Chiu. Four-dimensional data assimilation for coupled physical-acoustical fields. In N. G. Pace and F. B. Jensen, editors, *Acoustic Variability, 2002*, pages 417–424, Saclantcen, 2002. Kluwer Academic Press.

[30] P. F. J. Lermusiaux, C.-S. Chiu, and A. R. Robinson. Modeling uncertainties in the prediction of the acoustic wavefield in a shelfbreak environment. In E.-C. Shang, Q. Li, and T. F. Gao, editors, *Proceedings of the 5th International conference on theoretical and computational acoustics*, pages 191–200. World Scientific Publishing Co., May 21-25 2002.

[31] Pierre F. J. Lermusiaux, Jinshan Xu, Chi-Fang Chen, Sen Jan, L.Y. Chiu, and Yiing-Jang Yang. Coupled ocean–acoustic prediction of transmission loss in a continental shelfbreak region: Predictive skill, uncertainty quantification, and dynamical sensitivities. *IEEE Journal of Oceanic Engineering*, 35(4):895–916, October 2010.

[32] Y.-T. Lin, Timothy F. Duda, and Arthur E. Newhall. Three-dimensional sound propagation models using the parabolic-equation approximation and the split-step fourier method. *J. of Computational Acoustics*, 21(01):1250018, 2013.

[33] Ying-Tsong Lin, Jon M. Collis, and Timothy F. Duda. A three-dimensional parabolic equation model of sound propagation using higher-order operator splitting and pad approximants. *JASA*, 132(5):EL364–EL370, 2012.

[34] Ying-Tsong Lin, Timothy F. Duda, and Arthur E. Newhall. Three-dimensional sound propagation models using the parabolic-equation approximation and the split-step fourier method. *J. of Computational Acoustics*, 21(01):1250018, 2013.

[35] T. Lolla and P. F. J. Lermusiaux. A Gaussian mixture model smoother for continuous nonlinear stochastic dynamical systems: Applications. *MWR*, 145:2763–2790, July 2017.

[36] T. Lolla and P. F. J. Lermusiaux. A Gaussian mixture model smoother for continuous nonlinear stochastic dynamical systems: Theory and scheme. *MWR*, 145:2743–2761, July 2017.

[37] Larry Mayer, Martin Jakobsson, Graham Allen, Boris Dorschel, Robin Falconer, Vicki Ferrini, Geoffroy Lamarche, Helen Snaith, and Pauline Weatherall. The nippon foundation GEBCO seabed 2030 project: The quest to see the worlds oceans completely mapped by 2030. *Geosciences*, 8(2):63, 2018.

[38] Walter Munk, Peter Worcester, and Carl Wunsch. *Ocean acoustic tomography*. Cambridge university press, 2009.

[39] Chaim Leib Pekeris. Theory of propagation of explosive sound in shallow water. *Geol. Soc. Am. Mem.*, 27, 1948.

[40] Michael B Porter. The kraken normal mode program. Technical report, Naval Research Lab Washington DC, 1992.

[41] Peter Edward Robins and Alan G Davies. Morphological controls in sandy estuaries: the influence of tidal flats and bathymetry on sediment transport. *Ocean Dynamics*, 60(3):503–517, 2010.

[42] A. R. Robinson and P. F. J. Lermusiaux. Prediction systems with data assimilation for coupled ocean science and ocean acoustics. In A. Tolstoy et al, editor, *Proceedings of the Sixth International Conference on Theoretical and Computational Acoustics*, pages 325–342. World Scientific Publishing, 2004.

[43] David T Sandwell, R Dietmar Müller, Walter HF Smith, Emmanuel Garcia, and Richard Francis. New global marine gravity model from cryosat-2 and jason-1 reveals buried tectonic structure. *Science*, 346(6205):65–67, 2014.

[44] David T Sandwell, Walter HF Smith, Sarah Gille, Ellen Kappel, Steven Jayne, Khalid Soofi, Bernard Coakley, and Louis Géli. Bathymetry from space: Rationale and requirements for a new, high-resolution altimetric mission. *Comptes Rendus Geoscience*, 338(14-15):1049–1062, 2006.

[45] Themistoklis P. Sapsis and Pierre F. J. Lermusiaux. Dynamically orthogonal field equations for continuous stochastic dynamical systems. *Physica D: Nonlinear Phenomena*, 238(23–24):2347–2360, December 2009.

[46] Themistoklis P. Sapsis and Pierre F. J. Lermusiaux. Dynamical criteria for the evolution of the stochastic dimensionality in flows with uncertainty. *Physica D: Nonlinear Phenomena*, 241(1):60–76, 2012.

[47] NK Saxena, Atanu Basu. A review of shallow-water mapping systems. *Marine Geodesy*, 22(4):249–257, 1999.

[48] T. Sondergaard and P. F. J. Lermusiaux. Data assimilation with Gaussian Mixture Models using the Dynamically Orthogonal field equations. Part II: Applications. *Monthly Weather Review*, 141(6):1761–1785, 2013.

[49] T. Sondergaard and SapsisP. F. J. Lermusiaux. Data assimilation with Gaussian Mixture Models using the Dynamically Orthogonal field equations. Part I: Theory and scheme. *Monthly Weather Review*, 141(6):1737–1760, 2013.

[50] Frédéric Sturm. Numerical study of broadband sound pulse propagation in three-dimensional oceanic waveguides. *JASA*, 117(3):1058–1079, 2005.

[51] Frédéric Sturm and John A. Fawcett. On the use of higher-order azimuthal schemes in 3-d pe modeling. *JASA*, 113(6):3134–3145, 2003.

[52] F. D. Tappert. The parabolic approximation method. In J. B. Keller and J. S. Papadakis, editors, *Wave Propagation and Underwater Acoustics*, volume 70 of *Lecture Notes in Physics, Berlin Springer Verlag*, page 224, 1977.

[53] Alexandra Tolstoy. *Matched field processing for underwater acoustics*. World Scientific, 1993.

[54] M. P. Ueckermann, P. F. J. Lermusiaux, and T. P. Sapsis. Numerical Schemes and Studies for Dynamically Orthogonal Equations of Stochastic Fluid and Ocean Flows. MSEAS Report 11, Department of Mechanical Engineering, Massachusetts Institute of Technology, Cambridge, MA, 2011.

[55] Anne-Cathrin Woelfl, Helen Snaith, Sam Amirebrahimi, Colin Devey, Boris Dorschel, Vicki Ferrini, Veerle AI Huvenne, Martin Jakobsson, Jennifer Jencks, Gordon Johnston, et al. Seafloor mapping–the challenge of a truly global ocean bathymetry. *Frontiers in Marine Science*, 6:283, 2019.